Al-Kitab Journal for Pure Sciences (2026); 10(1):63-77.
https://doi.org/10.32441/kjps.10.1.p5

Al-Kitab Journal for Pure Sciences
ISSN: 2617-1260 (print), 2617-8141(online)

https://isnra.net/index.php/kjps

Preparation and Study the Properties of Ni-Co Ferrite Substituted with Ag- ions Calcined at 1000°C

Amal Khalaf Salim[1*], Sabah M. Ali Ridha[2], Asmaa Ahmad Aziz[3]

amal-Khalaf@uokirkuk.edu.iq[1], sabahyagmur@uokirkuk.edu.iq[2], asmaa.jamal@tu.edu.iq[3]

College of Education for Pure Science, University of Kirkuk, Iraq[1], College of Education for Pure Science, University of Kirkuk, Iraq[2], College of Education for Pure Science, University of Tikrit, Iraq[3].

[*]Corresponding Author: amal-Khalaf@uokirkuk.edu.iq

Citation: ***Amal Khalaf Salim[1*], Sabah M. Ali Ridha[2], Asmaa Ahmad Aziz[3]*** **.Preparation and Study the Properties of Ni-Co Ferrite Substituted with Ag- ions Calcined at 1000°C**.Al-Kitab J. Pure Sci. [Internet]. 2026 Apr 06; 10(1):63-77 DOI:

https://doi.org/10.32441/kjps.10.01.p5

Keywords: Sol-gel method, Dielectric properties, Silver-cobalt ferrite nanoparticles, Spinel ferrites, X-ray diffraction.

Article History

Received	13 Feb. 2025
Accepted	06 Apr. 2025
Available online	01 May. 2026

Abstract:

Analysis of the structural and dielectric properties of Ag-substituted Ni-Co spinel ferrite, represented by the formula $Ni_{0.4}Co_{(0.6-x)}Ag_{2x}Fe_2O_4$, were examined for values of (٠.00 ≥ X ≤ 0.45). An auto-combustion sol-gel process was used to synthesis this ferrite, which was then calcined at temperatures up to (1000°C). The ferrite samples underwent X-ray diffraction (XRD) research to determine their particle size, lattice characteristics, bulk density, and hopping length. The size of the crystallites varied between (32.952 nm and 43.926 nm), while the lattice parameter rose between 8.291 and 8.326 Å as the amount of silver ions increased. The X-ray density increased from 5.466 to 5.904 g/cm³, which was attributed to the larger molecular mass of silver (Ag) at 107.87 g/mol compared to cobalt (Co) at 58.93 g/mol.Dielectric properties were also studied, including both the real (ε') and imaginary (ε'') components of the dielectric constant, the dielectric loss represented by the loss tangent (tan δ), and electrical resistivity(ρ_{ac}). The results showed a decrease in both the real and imaginary dielectric constants, as well as a reduction in dielectric loss with increasing applied frequency. Additionally, a decrease in electrical resistivity was observed with increasing frequency.

Keywords: Sol-gel method, Dielectric properties, Silver-cobalt ferrite nanoparticles, Spinel ferrites, X-ray diffraction.

تحضير ودراسة خصائص فرايت النيكل-كوبالت المعوض بأيونات الفضة والمكلسنة عند ١٠٠٠°C

أمل خلف سالم[1*]، صباح محمد علي رضا[2]، أسماء احمد عزيز[3]

كلية التربية للعلوم الصرفة–جامعة كركوك– العراق، كلية التربية للعلوم الصرفة–جامعة كركوك– العراق، كلية التربية للعلوم الصرفة– جامعة تكريت– العراق.

amal-Khalaf@uokirkuk.edu.iq, sabahyagmur@uokirkuk.edu.iq, asmaa.jamal@tu.edu.iq

الخلاصة:

يدرس هذا البحث الخصائص التركيبية والعزلية لفرايت الكوبلت - الفضة، ذات الصيغة: $Ni_{0.4}Co_{(0.6-x)}Ag_{2x}Fe_2O_4$ حيث ان $(0.00 \geq X \leq 0.45)$ باستخدام طريقة السول-جل، حيث تم تلدين النماذج عند درجات حرارة تصل إلى ($1000°C$). ويدرس البحث ايضا الخواص التركيبية للعينات المحضرة باستعمال فحص حيود الأشعة السينية ((XRD) لتحديد حجم الجسيمات، وخصائص الشبكة البلورية، والكثافة الحجمية، وطول القفزات. حيث تراوح حجم البلورات بين ٣٢,٩٥٢ نانومتر و٤٣,٩٢٦ نانومتر، بينما زادت معامل الشبكية من ٨,٢٩١ إلى ٨,٣٢٦ $Å$ مع زيادة تركيز أيونات الفضة. كما أظهرت نتائج تحليل حيود الأشعة السينية زيادة في كثافة الأشعة السينية من ٥,٤٦٦ إلى ٥,٩٠٤ جرام/سم^3، ويرجع ذلك إلى الكتلة الجزيئية الأكبر للفضة (Ag) مقارنة بالكوبلت(Co) ، وتمت دراسة الخواص الكهربائية أيضًا، المتمثلة ثابت العزل الكهربائي بنوعيه الحقيقي (ε') والخيالي(ε'') ، بالإضافة إلى زاوية فقدان العزل $(tan\ \delta)$ والمقاومية الكهربائية(ρ_{AC}) . أظهرت النتائج انخفاضًا في كل من الثابت العازل الحقيقي والتخيلي، فضلًا عن انخفاض في فقدان العزل مع زيادة التردد المطبق. كما لوحظ انخفاض في المقاومية الكهربائية مع زيادة التردد.

الكلمات المفتاحية: طريقة السول-جل، الخصائص العزلية، الفرايت الكوبلت - الفضة النانوي، الفرايت الاسبينل، حيود الأشعة السينية(XRD).

1. Introduction:

A notable group of electrical materials, spinel ferrites are used in radio frequency circuits, factor gadgets of superior quality, cores of transformers, medium for magnetic recording, fluids that are magnetic, and other state-of-the-art technology because of their strong electrical resistance and minimal eddy current losses [1,2,3].Cobalt ferrite nanoparticles demonstrate improved characteristics when integrated with noble metals such as silver (Ag) or gold (Au). The incorporation of silver into Co-$NiFe_2O_4$ is anticipated to augment its antimicrobial efficacy owing to the intrinsic antibacterial characteristics of silver[4,5]. The characteristics of these ferrites are affected by various factors, such as the preparation technique, sintering parameters, chemical composition, crystallite dimensions, and the distribution of cations in the tetrahedral

(A) and octahedral (B) lattice sites, represented chemically by the formula AB_2O_4 [6,7,8,9]. Among ferrite materials, nanoparticles of cobalt and silver stand out for their high electrical resistance, low tangent losses, and excellent dielectric properties. Therefore, that is critical to investigate their dielectric characteristics throughout a range of frequencies[10,11]. This research intends to examine the impact of integrating silver ions into the cobalt ferrite structure on its electrical properties. This is accomplished by examining the real (ε') and imaginary (ε'') components of the dielectric constant, the dielectric loss tangent (tan δ), and the electrical resistivity (ρ_{ac}) across an extensive frequency spectrum. This work enhances the comprehension of the correlation between structural composition and electrical qualities, aiding in the creation of materials with improved electrical performance for advanced technological applications. These applications encompass supercapacitors, insulating materials in integrated circuits, electrical sensors, high-frequency transformers, electromagnetic wave-absorbing materials, and electronic components utilized in wireless communication and microwave technologies[12].

2. Material and methods:

Sol-gel technique was used to prepare six distinct samples of $Ni_{0.4}Co_{(0.6-x)}Ag_{2x}Fe_2O_4$, with the value of x ranging from 0.00 to 0.45. Initially, the solution was prepared using a set of pure chemicals, such as iron nitrate ($Fe(NO_3)_3 \cdot 9H_2O$), cobalt nitrate ($Co(NO_3)_2 \cdot 6H_2O$), silver nitrate ($Ag(NO_3)$), nickel nitrate ($Ni(NO_3)_2 \cdot 6H_2O$), and citric acid ($C_6H_8O_7 \cdot H_2O$). These materials were carefully chosen, as the metal nitrates act as oxidizing agents, while citric acid serves as a reducing agent, helping to form the final ferrite structure. Double distilled water was used throughout all experiments to ensure the solvent was free of impurities that could affect the reaction[13]. Subsequent to the solution's preparation, the mixture was incrementally heated on a hot plate to 90°C for two hours, culminating in the formation of a dense gel. Continuous agitation during this phase was essential to guarantee the uniform distribution of the components within the mixture. As the solvent evaporated, the mixture became increasingly concentrated, evolving into a viscous brown gel, which serves as the precursor to the self-propagating combustion process[14].

The next step, the temperature was increased to 250°C to initiate the self-combustion process, which removed the remaining water from the mixture and produced the burned ferrite powder. To ensure a fine and uniform powder, it was ground using a mortar and stirring mechanism, which helped improve the uniformity of the particles. The resultant powder was further heated to 400°C for three hours to eliminate any residual organic compounds and to enhance the

sample's homogeneity. Subsequently, the powder was combined with polyvinyl alcohol (PVA) as a binder to fabricate circular discs of 13 mm in diameter and roughly 2 mm in thickness. The dry pressing process involved applying a pressure of 3 tons using a hydraulic press for one minute to form the discs. The resultant discs were sintered at 1000°C for three hours to enhance the characteristics of the samples. Subsequent to the sintering procedure, the discs were allowed to cool naturally to ambient temperature, so preparing them for the examination of their insulating qualities. An electrical impedance analyzer was employed to assess these properties subsequent to the sintering of the samples **[15]** . **Figure1**shows the steps involved in using the sol-gel method for preparation **[16]**.

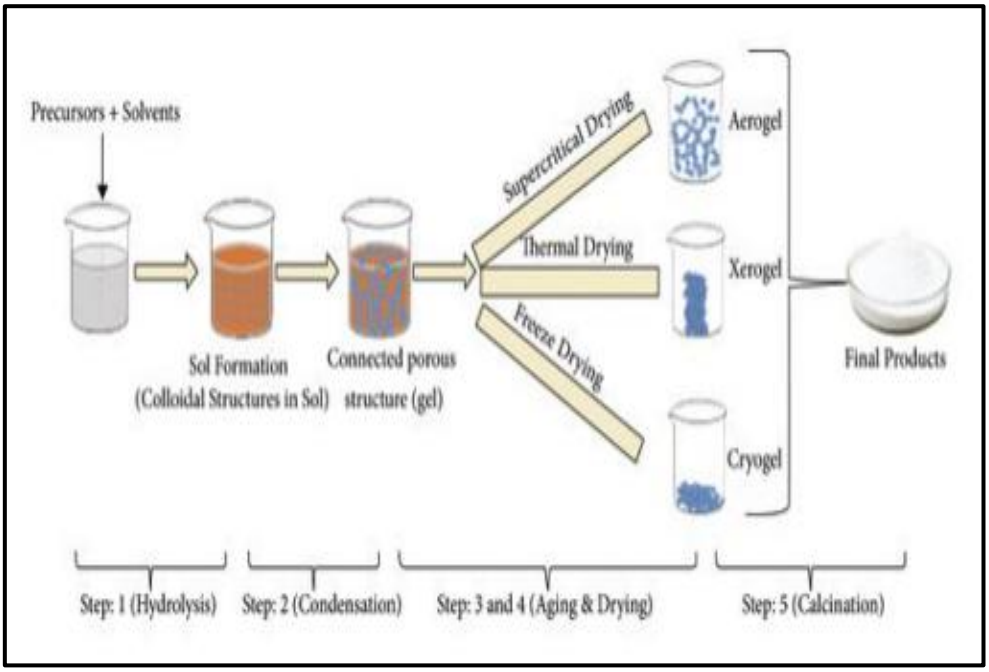

Figure1:Flowchart depicting the different phases of the so1-ge1 process: from precursor to aerogel (16)

3. X-ray diffraction analysis:

Figure 2 illustrates the XRD pattern for a sample with minimal Ag doping (x = 0. 00, 0.05, 0.15,0.25,0.35 and 0.45). The lattice planes (111), (220), (311), (222), (400), (422), (511), (440), (620), (533), and (622) exhibit various configurations. The material exhibits a single-phase spinel structure, with the most prominent diffraction peak found at the (311) plane. The cubic spinel structure (ICDD 22-1086) matches the indexed peaks corresponding to the lattice planes According to **[17]**. The crystallite size (D) of the samples was calculated based on the Debye-Scherrer equation **[18]**.

$$D = \frac{k\lambda}{(\beta\, Cos\theta)} \dots\dots\dots\dots\dots\dots\dots\dots\dots\dots\dots\dots\dots\dots (1)$$

In this context, β signifies the full width at half maximum (FWHM) in radians, k indicates the form factor, which is set at 0.89, λ is the wavelength of the incident X-ray beam, and its value is 0.15406 nm, and θ represents the Bragg diffraction angle[19].

The lattice constant (a) of the cubic spinel structure was ascertained using the approach.

$$a = d\sqrt{h^2 + k^2 + l^2} \dots\dots\dots\dots\dots\dots\dots\dots\dots\dots\dots\dots (2)$$

In this context, h, k, l denote Miller indices, while d represents interplanar distance, which may be calculated using Bragg's law: 2d sin θ = λ

Variations in the lattice parameter as a result of silver ion accumulation. The following equation is used to determine the X-ray density of the ferrite nanoparticles that are produced [20]:

$$\rho x = \frac{8M}{N_A a^3} \dots\dots\dots\dots\dots\dots\dots\dots\dots\dots\dots\dots\dots\dots (3)$$

M denotes the molecular weight, α marks the lattice parameter, and N_A represents Avogadro's number.

The hopping length at the tetrahedra1 (A) site and octahedra1 (B) site is determined using the subsequent equations [21].

$$L_A = a\frac{\sqrt{3}}{4} \dots\dots\dots\dots\dots\dots\dots\dots\dots\dots\dots\dots\dots\dots (4)$$

$$L_B = a\frac{\sqrt{2}}{4} \dots\dots\dots\dots\dots\dots\dots\dots\dots\dots\dots\dots\dots\dots (5)$$

The structural properties were computed utilizing the aforementioned equation, as indicated with in **Table 1**

Table 1: X-ray diffraction (XRD) results for $Ni_{0.4}Co_{(0.6-x)}Ag_{2x}Fe_2O_4$ ferrite nanoparticles calcined at 1000 °C.

x	D(nm)	a (Å)	ρ (g/cm³)	L_A(Å)	L_B(Å)
0.00	32.952	8.291	5.466	3.590	2.932
0.05	39.165	8.303	5.499	3.596	2.936
0.15	39.771	8.302	5.614	3.595	2.937
0.25	43.929	8.308	5.715	3.598	2.938
0.35	43.928	8.323	5.797	3.604	2.943
0.45	43.926	8.326	5.904	3.605	2.944

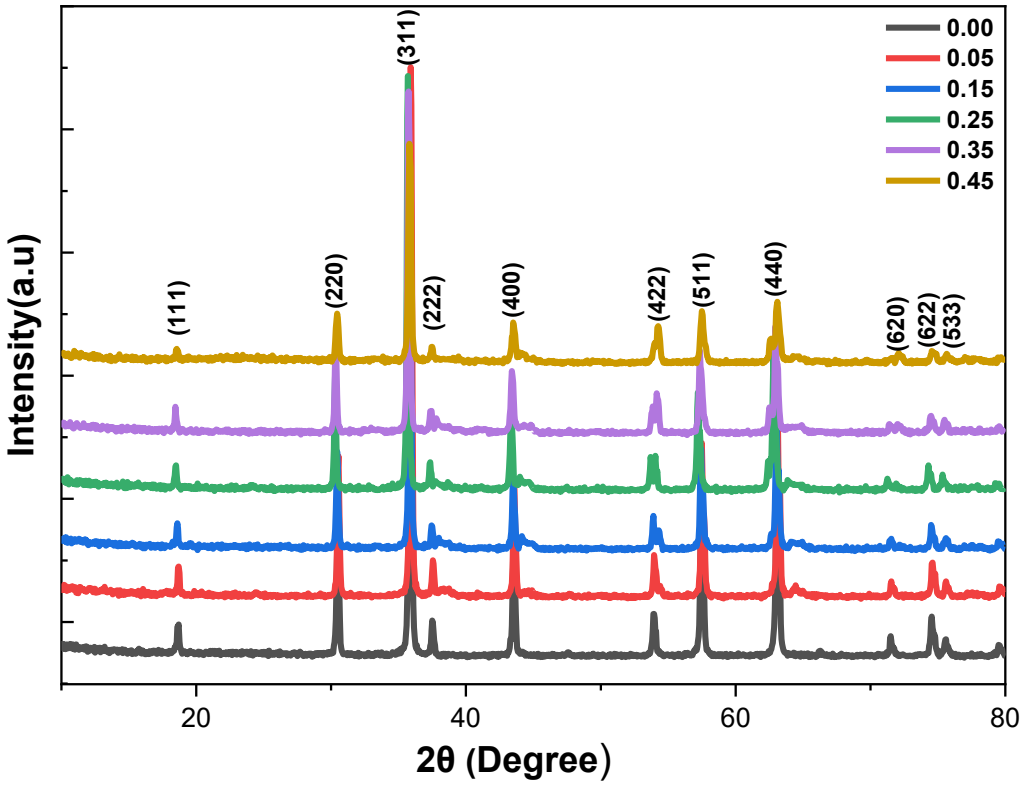

Figure 2: XRD pattern of nanoparticles $Ni_{0.4}$ Co $_{(0.6-x)}$ $Ag_{2x}FeO_{42}$.

3.1 Crystallite Size (D):

Equation 1 and X-ray diffraction (XRD) analysis were used to determine the crystallite size (D). The 311) peak and its full width at half maximum (FWHM) as well as its peak position (2θ) were used for the measurements. For the $Ni_{0.4}Co_{(0.6-x)}Ag_{2x}Fe_2O_4$ ferrites at 1000°C, the particle sizes, depending on the varying x concentrations, ranged from 32.952 nm to 43.926 nm, as presented in **Table 1.** The results indicated that the crystallite size increases with the enhancement of silver doping in Ni-$CoFe_2O_4$, as the higher concentration of Ag^+ ions substituting Co^{2+} ions leads to a larger crystallite size. This increase is attributed to the larger ionic radius of Ag^+ (1.26 Å) compared to Co^{2+} (0.83 Å) ,and Fe^{2+} (0.92 Å) ions, This is consistent with the researchers' results **[22,23]**. As the silver concentration (x) increases in the crystal lattice, the available sites in the crystal structure are filled with silver ions. However, after a certain concentration (typically at X = 0.25 or higher), the network reaches a state of "saturation," where most of the sites in the lattice are fully occupied. Therefore, silver can no longer significantly influence the expansion of the crystallite size beyond this point, leading to the stabilization of the crystallite size**[24]**.

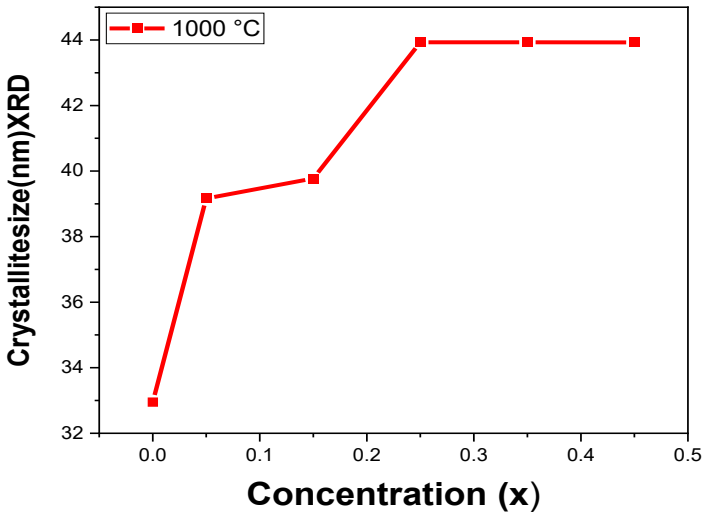

Figure 3: Variation in Crystallite Size (D) with Ag Concentration (x) for Ni-Co Ferrites Sintered at 1000°C.

3.2 Lattice Parameter (a):

The lattice parameter (a) for the sample at the (311) peak at 1000°C was calculated using **Equation 2**, and the results are shown in **Table 1**. As silver content increases, the lattice parameter of silver-cobalt ferrite go from 8.291 Å to 8.326 Å. According to the researchers, this is because the ionic radius of Ag^{+} (1.26 Å) is larger than that of Co^{2+} (0.83 Å). Consequently, the lattice constant of cobalt ferrite that is substituted with silver is expected to increase as the concentration of silver increases **[25,٢٦]**.

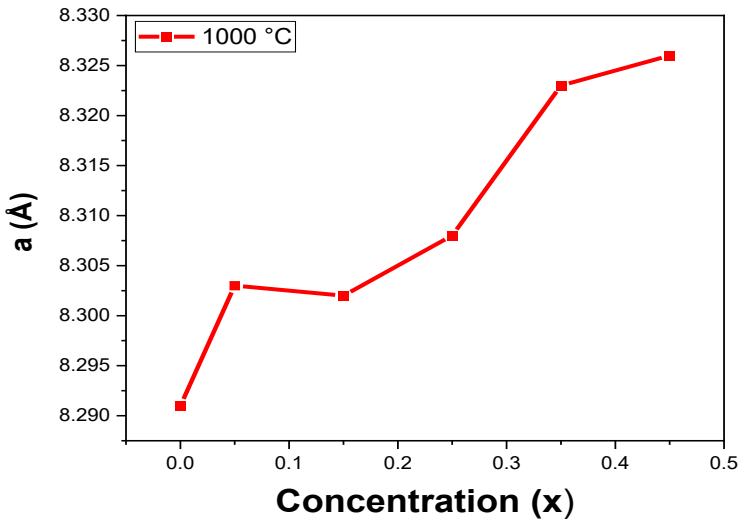

Figure 4: Lattice Parameter Variation as a Function of Ag Content (x) for Ni-Co Ferrites.

3. 3 Theoretical Density (ρ_x-ray):

Equation 3 was applied to determine the theoretical density values (ρx-ray) of the $Ni_{0.4}Co_{(0.6-x)}Ag_{2x}Fe_2O_4$ ferrite phase at 1000°C across various silver concentrations (x = 0.0 to 0.45). **Figure 5** depicts the relationship between silver concentration and density. The disparity in molar masses between cobalt (Co^{2+}) and silver (Ag^{+}) is responsible for the observed shift in behavior. Comparing silver to cobalt (Co), the former has a molar mass of 107.87 g/mol and the latter stands at 58.93 g/mol. The density is increased when silver is used in place of cobalt because silver has a larger atomic weight, This is consistent with the researcher results**[20]**.

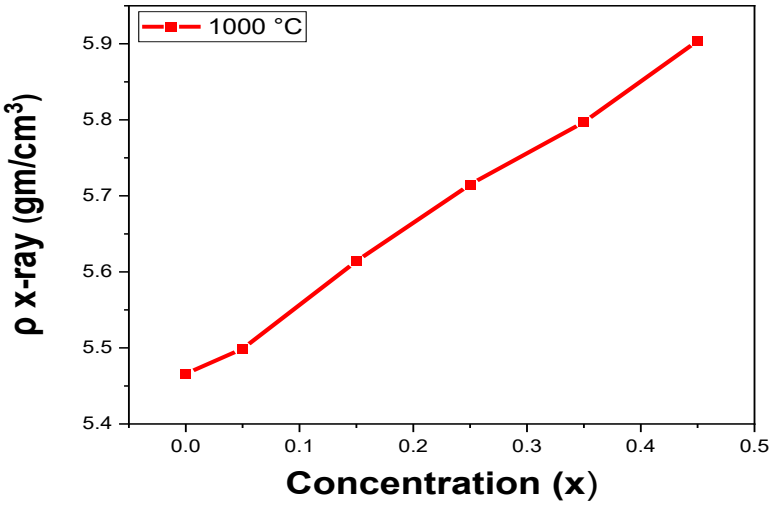

Figure 5: shows how the theoretical density values (ρ_x-ray) for Ni-Co ferrites vary with increasing Ag Content (x).

3. 4 Hopping Length (L):

The lengths of ion hop at the tetrahedra1 (A) site L_A and octahedra1 (B) site L_B were determined by calculating the interionic distances using the crystal lattice constant, as outlined in **Equations 4 and 5**. The calculated values for the synthesized Ag-Co ferrite sample at 1000°C are illustrated in **Figures ٦** and **Table 1**. It is evident that the ionic jump lengths increase with augmented Ag content. Given that silver ions are larger than cobalt ions, their substitution results in an expansion of the lattice constant, thereby yielding a denser crystal structure**[14].** The ionic jump lengths (L_A and L_B) exhibit a direct proportionality to the lattice constant (a), This results in a rise in jump lengths as silver concentrations increase. Furthermore, the ionic jump length (L_B) is somewhat shorter than (L_A) due to the more compact nature of the (L_B) sites, resulting in shorter jump distances; this is consistent with the researcher's results **[27,28]**.

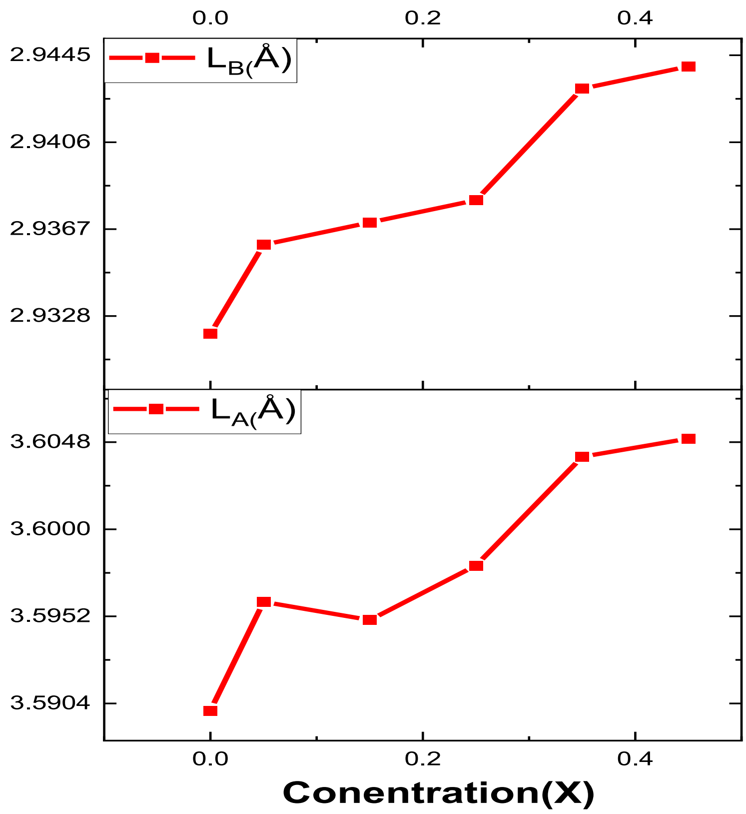

Figure ٦: Shows the variation in jump lengths L_A and L_B for Ni-Co ferrites with increasing Ag content (x).

4. Electrical Characteristics:

The behavior of nanoparticles made from ferrite demonstrates the mechanism associated with the dielectric response to alternating electric fields and electrical conduction processes. These properties are influenced by several factors, including chemical composition, manufacturing process, the ratio of components, particle size, ionic charge, porosity, and the cation distribution between the tetrahedra1 (A-site) and octahedra1(B-site) [29].

Calculations of the dielectric properties of the $Ni_{0.4}Co_{(0.6-x)}Ag_{2x}Fe_2O_4$ sample at room temperature were carried out, including the dielectric constant (ε′), dielectric loss (ε″), dielectric loss angle (tan δ), and electrical resistivity (ρ_{ac}) as a function of frequency (500kHz – 5MHz) using the following equations [30].

$$\varepsilon' = \frac{Cd}{\varepsilon_\circ A} \quad \text{……………………………………………………} (6)$$

$$tan\delta = \frac{1}{2\pi f R_P \; C_P} \quad \text{…………………………………………..}(7)$$

$$\varepsilon'' = \varepsilon' tan\delta \quad \text{……………………………………………} (8)$$

$$\rho = R_P \frac{A}{d} \dots\dots\dots\dots\dots\dots\dots\dots\dots\dots\dots\dots\dots\dots\dots (9)$$

In this context, C denotes the capacitance of the pellet in farads, d represents the thickness of the pellet in meters, A signifies the cross-sectional area of the pellet's flat surface, ε_o refers to the permittivity constant of free space, Rp indicates the equivalent parallel resistance, and Cp stands for the equivalent parallel capacitance, A Surface area of the insulator, and d Thickness of the insulator

Figure (7-10) Illustrates the variation of the dielectric constant (ε'), the dielectric loss angle (tan δ), dielectric loss factor (ε''), and the electrical resistivity (ρ_{ac}) as a function of frequency.

4.1 Dielectric Constant (ε'):

Figure ٧ shows how the real dielectric constant (ε') changes with frequency at ambient temperature, ranging from (50 Hz to 5 MHz) for $Ni_{0.4}Co_{(0.6-x)}Ag_{2x}Fe_2O_4$ ferrite samples. As the frequency increases, a decrease in the dielectric constant (ε') is observed, which can be explained by **Equation 6**. It can be inferred that the ferrite samples contain conductive grains with non-conductive grain boundaries. Electron polarization occurs when electrons hop across the non-conductive grain boundaries, where they accumulate due to the increased resistance. At higher frequencies, the electrons fail to interact with the oscillating field, minimizing the probability of electrons encountering the grain boundaries, hence diminishing polarization, This aligns with the researcher's findings **[31,32]**.

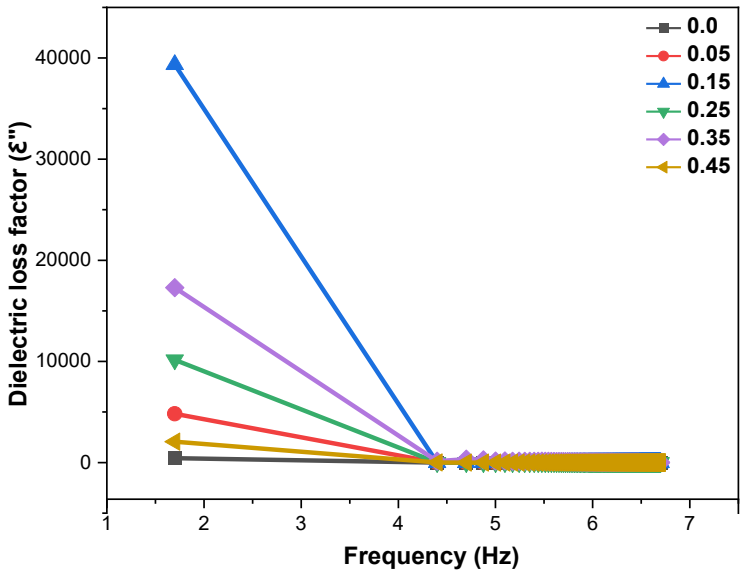

Figure 7:The dependence of dielectric constant (ε') on frequency for $Ni_{0.4}Co_{(0.6-x)}Ag_{2x}Fe_2O_4$.

4.2 Dielectric Loss Angle ($tan\delta$):

The values of tangent loss ($tan\delta$) are influenced by various elements, including chemical composition, Fe^{2+} concentration, and structural uniformity, all of which are contingent upon the composition of the ferrite samples and the calcination temperature.

Figure 8 illustrates the fluctuation of tangent loss relative to frequency for Ni-Co ferrite samples with varying silver ion (x) concentrations. The factor of dielectric loss is highest at low frequencies and declines with the rise in the applied electric field frequency, as explained by **Equation 7**. The inverse relationship between the dielectric loss factor and frequency arises from the substantial energy gained by dipoles from the applied electric field, which heightens the probability of collisions among these dipoles as they rotate at lower frequencies, resulting in diminished dielectric properties. With the increase in the applied field frequency, the capacity of the dipoles to track the fluctuations in the field diminishes, leading to a reduction in the energy absorbed by the dipoles from the applied field, and consequently, a decline in the dielectric loss factor, This is consistent with the researcher results **[33]**.

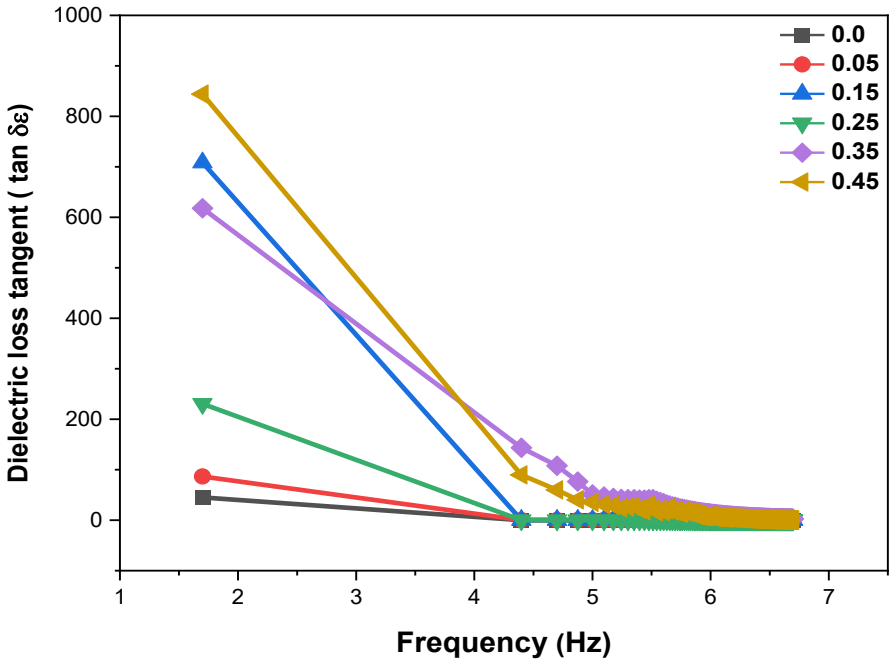

Figure 8: Displays the correlation between frequency and dielectric loss angle (tanδ) for spinel nanoparticles of $Ni_{0.4}Co_{(0.6-x)}Ag_{2x}Fe_2O_4$.

4.3 Dielectric Loss Factor (ε"):

The imaginary portion of the dielectric constant (ε″) representing the loss of dielectric energy, is calculated through **Equation 8** and is a critical parameter in evaluating the total core loss of ferrites. Consequently, lower dielectric losses are preferred for reducing core loss. The relationship between dielectric loss (ε″) and frequency for Ni-Co nano ferrite samples with different levels of Ag-ion content (x) is shown in **Figure 9**. The dielectric loss curve resembles the tangent loss shown in the previous figure. The increase in electron hopping results in a localized shift in the direction of the applied electric field, resulting in higher electric polarization and consequently enhancing the dielectric loss factor, This is consistent with the researcher's results **[31,34]**.

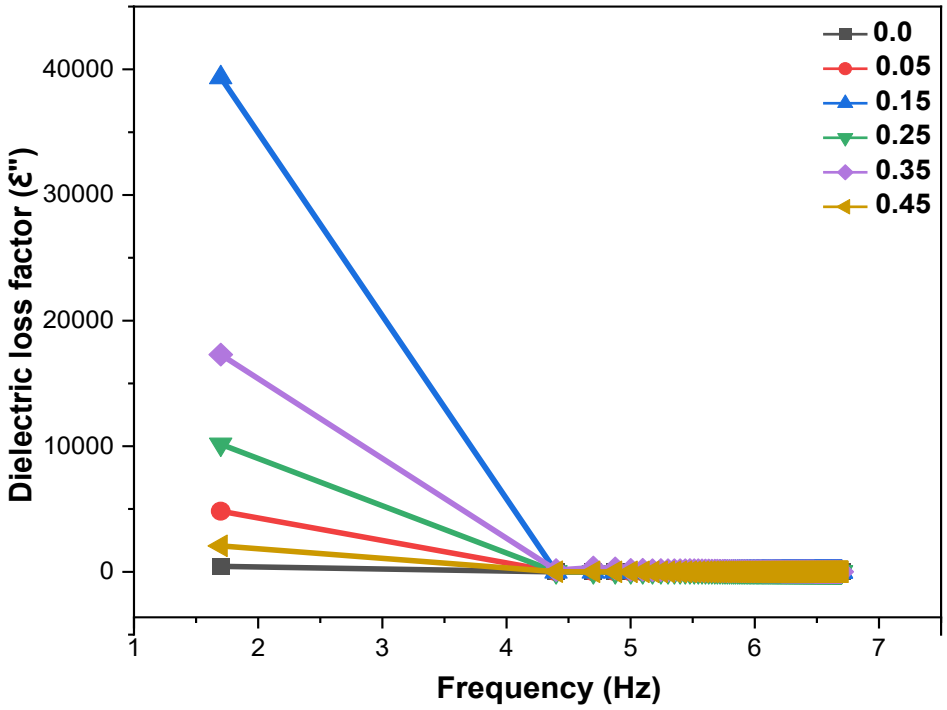

Figure 9: Relationship between the dielectric loss factor (ε′′) and frequency for $Ni_{0.4}Co_{(0.6-x)}Ag_{2x}Fe_2O_4$ spinel nanoparticles.

4.4 Resistivity (ρ_{ac}):

Using **Equation 9**, the electrical resistance was computed, where **Figure 10** shows the relationship between electrical resistance and frequency. As the frequency increases, a drop in electrical resistance is detected, following a pattern similar to the real value of the dielectric constant (ε′) and the imaginary component of dielectric loss (ε″). This tendency suggests that electrical conductivity rises with increasing frequency. This alteration can be described based

on the conduction mechanism in ferrite materials, where electron transfer happens between (Fe^{2+}) and (Fe^{3+}) ions at the octahedral locations (site B). As the ions get closer together, this transfer increases, leading to electron hopping in internal displacements, resulting in polarization. This is congruent with the researchers' results [35,34].

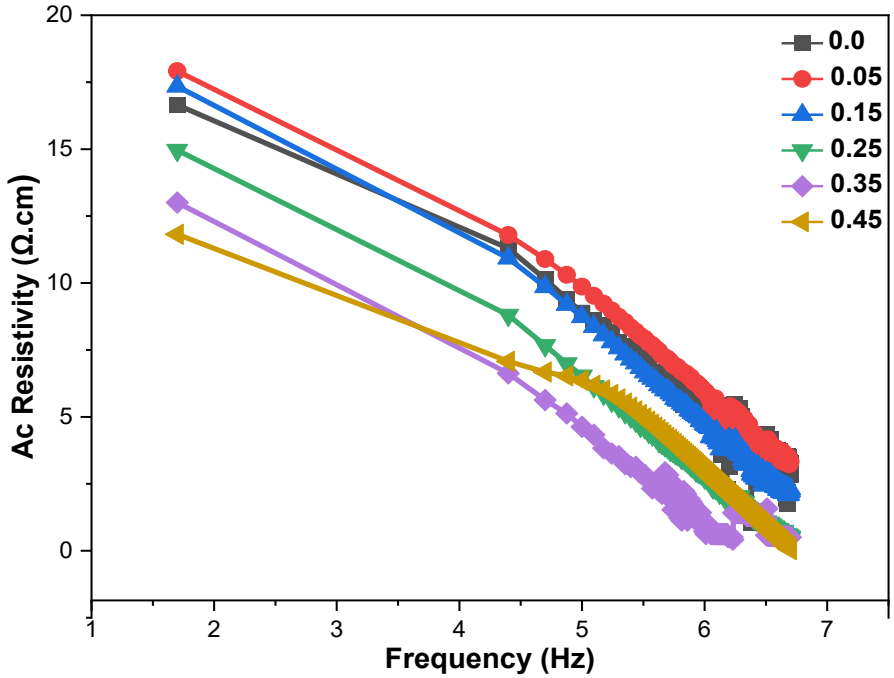

Figure 10: Resistivity (ρ_{ac}) variation with frequency for $Ni_{0.4}Co_{(0.6-x)}Ag_{2x}Fe_2O_4$ spinel nanoparticles.

5. Conclusions

This work studied the effect of substituting Co ion with Ag ion in the spinel ferrite structure $Ni_{0.4}Co_{(0.6-x)}Ag_{2x}Fe_2O_4$, synthesized using the auto-combustion so1-ge1 process and sintered at 1000°C. X-ray diffraction (XRD) studies demonstrated an increase in lattice constant and bulk density with increasing Ag content, which is due to the larger molecular mass of Ag. Dielectric investigations demonstrated a drop in both the real (ε′) and imaginary (ε″) components of the dielectric constant, as well as a reduction in dielectric loss (tan δ) and AC electrical resistivity (ρ_{ac}) with increasing frequency. These discoveries contribute to the understanding of the relationship between the structural composition and electrical properties of the material, supporting applications in high-frequency circuits, sensors, integrated circuit insulation, and electromagnetic wave absorption. Additionally, introducing Ag may boost the antibacterial capabilities, expanding its potential for medical and electrical applications. Overall, this work helps to the creation of high-performance materials appropriate for sophisticated technological applications.

6. References

[1] Ripka P. Magnetic sensors and magnetometers. Meas Sci Technol. 2002;13(4):645.
[2] Charles SW. The preparation of magnetic fluids. Ferrofluids Magn Control fluids their Appl. 2002;3–18.
[3] Sellmyer D, Skomski R. Advanced magnetic nanostructures. Springer; 2006.
[4] Shukla R, Ningthoujam RS, Umare SS, Sharma SJ, Kurian S, Vatsa RK, et al. Decrease of superparamagnetic fraction at room temperature in ultrafine CoFe 2 O 4 particles by Ag doping. In: ICAME 2007: Proceedings of the 29th International Conference on the Applications of the Mössbauer Effect (ICAME 2007) held in Kanpur, India, 14-19 October 2007. Springer; 2009. p. 631–9.
[5] Aziz C, Azhdar B. Synthesis of dysprosium doped cobalt ferrites nanoparticles by solgel auto-combustion method and influence of grinding techniques on structural, Morphological, and magnetic properties. J Magn Magn Mater. 2022;542:168577.
[6] Awati V V. Structural, dielectric and magnetic properties of Ni substitution in Cu-Zn nano ferrite. Int J Curr Res. 2013;5:2510–4.
[7] Balavijayalakshmi J, Suriyanarayanan N, Jayaprakash R. Role of copper on structural, magnetic and dielectric properties of nickel ferrite nano particles. J Magn Magn Mater. 2015;385:302–7.
[8] Pathan AT, Shaikh AM. Dielectric properties of Co-substituted Li-Ni-Zn nanostructured ferrites prepared through chemical route. Int J Comput Appl. 2012;45(21):975–8887.
[9] 9. Maheen M, Rafeekali K, Sebastian R, Mohammed EM. Structural and Dielectric Studies of Cerium Substituted Nickel Ferrite Nano Particle. Int J Eng Sci(IJES). 2015;4:33.
[10] Abbas T, Islam MU, Ashraf Ch M. Study of sintering behavior and electrical properties of Cu-Zn-Fe-O system. Mod Phys Lett B. 1995;9(22):1419–26.
[11] Ridha SMA. X-ray studies and electrical properties of the zinc-substituted copper nanoferrite synthesized by sol-gel method. Int J Compos Mater. 2015;5(6):195–201.
[12] Kaiser M. Effect of silver nanoparticles on properties of cobalt ferrites. J Electron Mater. 2020;49(8):5053–63.
[13] Dabagh S, Dini G. Synthesis of silica-coated silver-cobalt ferrite nanoparticles for biomedical applications. J Supercond Nov Magn. 2019;32(12):3865–72.
[14] Satheeshkumar MK, Kumar ER, Srinivas C, Suriyanarayanan N, Deepty M, Prajapat CL, et al. Study of structural, morphological and magnetic properties of Ag substituted cobalt ferrite nanoparticles prepared by honey assisted combustion method and evaluation of their antibacterial activity. J Magn Magn Mater. 2019;469:691–7.
[15] Mojić B, Giannakopoulos KP, Cvejić Ž, Srdić V V. Silica coated ferrite nanoparticles: Influence of citrate functionalization procedure on final particle morphology. Ceram Int. 2012;38(8):6635–41.
[16] Ashiq MGB. Structural, dielectric, morphological and magnetic properties of cobalt-substituted nickel spinel ferrites (CoxNi1-xFe2O4) nanoparticles. Appl Nanosci. 2023;13(6):4541–54.
[17] Purnama B, Wijayanta AT. Effect of calcination temperature on structural and magnetic properties in cobalt ferrite nano particles. J King Saud Univ. 2019;31(4):956–60.
[18] Kumar ER, Srinivas C, Seehra MS, Deepty M, Pradeep I, Kamzin AS, et al. Particle size dependence of the magnetic, dielectric and gas sensing properties of Co substituted NiFe2O4 nanoparticles. Sensors Actuators A Phys. 2018;279:10–6.
[19] Ghorbani H, Eshraghi M, Dodaran AAS, Kameli P, Protasowicki S, Vashaee D. Effect of Yb doping on the structural and magnetic properties of cobalt ferrite nanoparticles.

Mater Res Bull. 2022;147:111642.
[20] Kumar G, Rani R, Sharma S, Batoo KM, Singh M. Electric and dielectric study of cobalt substituted Mg Mn nanoferrites synthesized by solution combustion technique. Ceram Int. 2013;39(5):4813–8.
[21] Das S, Bououdina M, Manoharan C. The influence of cationic surfactant CTAB on optical, dielectric and magnetic properties of cobalt ferrite nanoparticles. Ceram Int. 2020;46(8):11705–16.
[22] Mahajan P, Sharma A, Kaur B, Goyal N, Gautam S. Green synthesized (Ocimum sanctum and Allium sativum) Ag-doped cobalt ferrite nanoparticles for antibacterial application. Vacuum. 2019;161:389–97.
[23] Lide DR. CRC handbook of chemistry and physics. Vol. 85. CRC press; 2004.
[24] Jauhar S, Kaur J, Goyal A, Singhal S. Tuning the properties of cobalt ferrite: A road towards diverse applications. RSC Adv. 2016;6(100):97694–719.
[25] Hossain AKMA, Kabir KK, Seki M, Kawai T, Tabata H. Structural, AC, and DC magnetic properties of Zn1− xCoxFe2O4. J Phys Chem Solids. 2007;68(10):1933–9.
[26] Riyatun R, Kusumaningsih T, Supriyanto A, Purnama B. Characteristics of the microstructure, magnetic and antibacterial properties of silver-substituted cobalt ferrite nanoparticles from the sol-gel method. Kuwait J Sci. 2023;50(4):569–74.
[27] Sridhar R, Dachepalli R, K Vijaya K. Synthesis and characterization of copper substituted nickel nano-ferrites by citrate-gel technique. Adv Mater Phys Chem. 2012;2012.
[28] Senthamilselvan T, Nithiyanantham S, Koteeshwari RS, Malarkodi B, Kogulakrishnan K, Lakshmigandhan T, et al. Studies on silver-doped magnesium ferrite utilizing the sol–gel process in terms of structure, magnetism, electricity, and electrochemistry. J Mol Struct. 2024;1311:138445.
[29] Mohammad AM, Ridha SMA, Mubarak TH. Dielectric properties of Cr-substituted cobalt ferrite nanoparticles synthesis by citrate-gel auto combustion method. Int J Appl Eng Res. 2018;13(8):6026–35.
[30] Pervaiz E, Gul IH. Enhancement of electrical properties due to Cr3+ substitution in Co-ferrite nanoparticles synthesized by two chemical techniques. J Magn Magn Mater. 2012;324(22):3695–703.
[31] Tamboli QY, Bushnak I, Patange SM, Zakde KR, Jadhav KM. Effect of Ag on dielectric, elastic, electrical impedance, and Raman spectroscopic properties of CoFe2O4. J Sol-Gel Sci Technol. 2025;1–10.
[32] Maxwell JC. A treatise on electricity and magnetism. Clarendon Press google Sch. 1873;2:3408–25.
[33] Yadav RS, Kuřitka I, Vilcakova J, Havlica J, Masilko J, Kalina L, et al. Impact of grain size and structural changes on magnetic, dielectric, electrical, impedance and modulus spectroscopic characteristics of CoFe2O4 nanoparticles synthesized by honey mediated sol-gel combustion method. Adv Nat Sci Nanosci Nanotechnol. 2017;8(4):45002.
[34] Sindhu S, Anantharaman MR, Thampi BP, Malini KA, Kurian P. Evaluation of ac conductivity of rubber ferrite composites from dielectric measurements. Bull Mater Sci. 2002;25:599–607.
[35] Nongjai R, Khan S, Asokan K, Ahmed H, Khan I. Magnetic and electrical properties of In doped cobalt ferrite nanoparticles. J Appl Phys. 2012;112(8).